The variation of PbTiO3 bandgap at ferroelectric phase transition

Article *in* Journal of Physics Condensed Matter · December 2015

DOI: 10.1088/0953-8984/28/2/025501

IOP Publishing Journal of Physics: Condensed Matter
J. Phys.: Condens. Matter **28** (2016) 025501 (8pp) doi:10.1088/0953-8984/28/2/025501

The variation of $PbTiO_3$ bandgap at ferroelectric phase transition

V Železný[1], D Chvostová[1], D Šimek[1], F Máca[1], J Mašek[1], N Setter[2] and Yu Hong Huang[2]

[1] Institute of Physics, Academy of Sciences of the Czech Republic, Na Slovance 2, 182 21 Prague 8, Czech Republic
[2] Ceramics Laboratory, EPFL-Swiss Federal Institute of Technology, Lausanne 1015, Switzerland

E-mail: zelezny@fzu.cz

Received 10 September 2015, revised 11 November 2015
Accepted for publication 23 November 2015
Published 17 December 2015

Abstract

Optical properties of the $PbTiO_3$ thin films fabricated by chemical solution deposition have been measured with variable angle spectroscopic ellipsometry in the spectral range of 1–6 eV and in the temperature interval from room temperature to 950 K. The optical response functions and band gap energy were determined in the whole temperature range. The direct band gap varies from the value 3.88 eV at room temperature to the value 3.67 eV just above the phase transition. The temperature dependence of the film lattice parameters was also measured by x-ray and it shows a strong correlation with the band gap. The comparison of experimental data with *ab initio* electronic structure calculations simulating the temperature development of dielectric function and band gap is also presented.

Keywords: band gap, ellipsometry, ferroelectrics

(Some figures may appear in colour only in the online journal)

1. Introduction

Perovskite materials are of interest from several points of view [1–4]. First, some of these materials are widely used as substrates for the growth of high-T_c superconductors and colossal magnetoresistance thin films. Second, these materials are of enormous importance for applications that make use of their unusual piezoelectric, ferroelectric, and dielectric properties for piezoelectric transducers, non-volatile memories, and wireless communication applications, and recently increasing interest is in the semiconducting form for photonics materials. Third, the materials display a variety of structural phase transitions: the ferroelectric, antiferroelectric and antiferrodistortive transitions and especially their microscopic mechanism is of considerable fundamental interest. $PbTiO_3$ in itself has been often and intensively studied as an end member of the solid solution system $Pb(Zr/Ti)O_3$ (PZT), which is the most used ferroelectric material for technical applications usually in the form of ceramics or thin films.

$PbTiO_3$ is considered as the simplest of these materials and a textbook example of a displacive ferroelectric transition [5, 6]. It undergoes a clearly established first-order transition at 493 °C (766 K) from cubic $Pm\bar{3}m$ (O_h^1) (parent perovskite) to a tetragonal ferroelectric phase. At room temperature the structure has the space group $P4\,mm$ (C_{4v}^1), with a tetragonal distortion c/a of 1.064. The displacement of the Ti and O ions relative to Pb and parallel to the polar axis is 17 pm and 47 pm, respectively [7]. The changes of the crystallographic parameters associated with this transition are large enough to be reliably determined.

Despite the simplicity of the $PbTiO_3$ phase transition, the experimental study of the bulk material is hampered by high electrical conductivity and difficulty in growing single crystals due to the first order character of the phase transition and large tetragonal distortion that occurs at it. Both quantities show abrupt discontinuities typical of first-order transition [6]. As a result not all these characteristics including the thermodynamics classification are completely known [6] and especially on a microscopic level they are not yet fundamentally understood [8].

First-principle calculations based on density functional theory (DFT) were applied to elucidate microscopic behavior and stability of ferroelectrics. They were used to calculate and

compare the total energy for particular phases or to calculate polarization, piezoelectric parameters of phonons and to study their energy surfaces and phase diagrams (see e.g. [9] and references therein).

In this paper, we investigate polycrystalline $PbTiO_3$ thin films prepared by chemical solution deposition (CSD) on sapphire (Al_2O_3) substrates. Using spectroscopic ellipsometry we determined the temperature dependence of their optical response functions and electronic band gap. We also measured lattice parameters by x-ray diffraction (XRD) and the positions of atoms in the unit cell as a function of temperature. The structural and optical properties were studied from room temperature to 950 K with special interest in the vicinity of the phase transition at 766 K. The structural data were used as an input for the first-principle calculations to simulate the temperature development of the electronic structure and optical properties. We did not calculate the electronic and optical properties only in the cubic and tetragonal phases, but using the structural data at various temperatures we simulated the direct influence of structure geometry on the electronic structure of this system. The calculations show the existence of local distortion even in the quasi-cubic phase (with lattice parameters $a = c$) resulting in shifting ions into off-center positions. We show here that this distortion must be taken into account to explain the temperature dependence of the band gap. It also indicates that the phase transition might be a result of a combined action of local distortion and ion displacement.

2. Experimental

To avoid the problems connected with the sample destruction when $PbTiO_3$ passes through the phase transition, for our experiment we used polycrystalline thin films prepared by CSD technique using lead acetate trihydrate and Ti-isopropoxide. Pyrolysis was done at 450–500 °C and final annealing of the film was at 600–700 °C. Further details can be found in [10]. The film was of 0.8 μm thickness and deposited on 0.54 mm thick sapphire (Al_2O_3) substrate.

The structure of the $PbTiO_3$ thin films was investigated by XRD using two different experimental setups: parallel beam diffractometer (Cu $K_\alpha = 0.1541$ nm) and Panalytical X'pert Bragg–Brentano goniometer. The variable angle spectroscopic ellipsometry (VASE) was used to investigate the optical properties and to determine the dielectric function of the $PbTiO_3$ thin films. The measurements were carried out using a standard VASE (Woollam, Inc.) spectrometer working in a rotating analyzer mode in the spectral range 1–6 eV and at incidence angles 65, 70 and 75° at room temperature. The high temperatures (RT - 950 K) spectra were taken at one incidence angle 70° in a home-made oven.

3. Experimental results

3.1. X-ray determination of structure parameters

The temperature dependent XRD measurements were carried out on a Panalytical X'Pert theta-theta goniometer equipped with a position sensitive detector X'celerator. The incoming and outgoing angles were kept equal to maintain the semi-focusing geometry. The data were acquired in a 2θ range from 20 to 120 degrees with 0.05 step size using CoK_α radiation ($\lambda_1 = 0.178\,901$ nm, $\lambda_2 = 0.179\,290$ nm with 2:1 intensity ratio). The XRD results show that the films in our study were well-grown polycrystalline with a pure perovskite structure.

The analysis was performed by means of Rietveld type refinement using a routine described in [11] with a correction for a fiber-like texture. Tetragonal $PbTiO_3$ was taken as a structural model; the refined parameters were the lattice constants a and c, the occupancies of titanium and lead atoms, z-positions of titanium and oxygen and isotropic thermal displacements of all atoms. The precision of these parameters except the lattice constant is poor due to the correlation with texture and absorption corrections, but it allows a good fit of the calculated diffraction pattern to the experimental one in order to obtain lattice constants a and c precisely. In the cubic phase above the transition temperature the refined parameters a and c yield an equal value. The temperature dependence of the lattice parameters is shown in figure 3(b). Our lattice parameters and their temperature dependence are in good agreement with bulk data [6, 12]. The c/a ratio deviation of our data and those on a single crystal is less than 0.5% at room temperature.

The texture of $PbTiO_3$ was found to be weak fibre of 001 pole having maximum normal to the surface. The 50% intensity of 00l reflections with respect to the maximum was at about 60 degrees inclination from the surface normal.

3.2. Ellipsometric determination of optical functions

Optical absorption across the direct gap in perovskites is strong and their optical properties can be very precisely determined using VASE. The ellipsometric angles Ψ and Δ of the $PbTiO_3$ thin films were measured as a function of frequency from 1 to 6 eV and angle of incidence at 60, 65 and 70°. The measured and fitted ellipsometric functions Ψ and Δ for the selected angle of incidence 70° are presented in figure 1, where their very good coincidence can be clearly seen. The remaining data at the other incidence angles were omitted for simplicity and clarity of the figure.

At first sight it is seen that the spectra in figure 1 can be divided in a region of a strong absorption due to interband electronic transitions and a transparent region characterized by interference oscillations coming from multiple reflection from the upper and bottom interfaces of the thin film. The boundary between both regions located approximately at 3.8 eV determines the band gap.

For extracting the film response functions from the experimental data a standard transfer matrix technique with matrices for each layer was used to generate model data and to fit them to the experiment. The structural model for the simulation of our experimental data consisted of four layers: top surface roughness / $PbTiO_3$ film / intermix / Al_2O_3 substrate. The Al_2O_3 substrate was measured independently and its optical response was calculated using the Drude–Lorentz model. The real $n(E)$ and imaginary $k(E)$ parts of its refractive index obtained in this way were in good agreement with the data

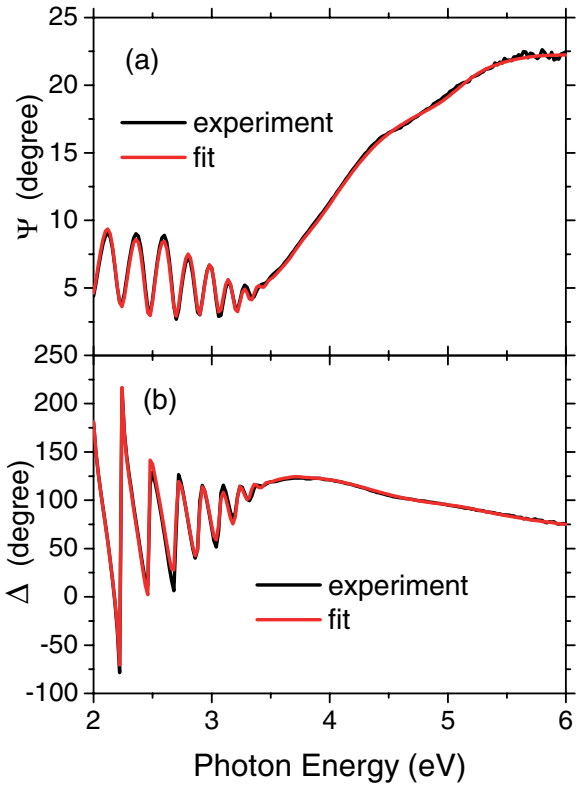

Figure 1. The experimental ellipsometric angles Ψ and Δ at room temperature compared with model calculation refined by point-to-point calculation.

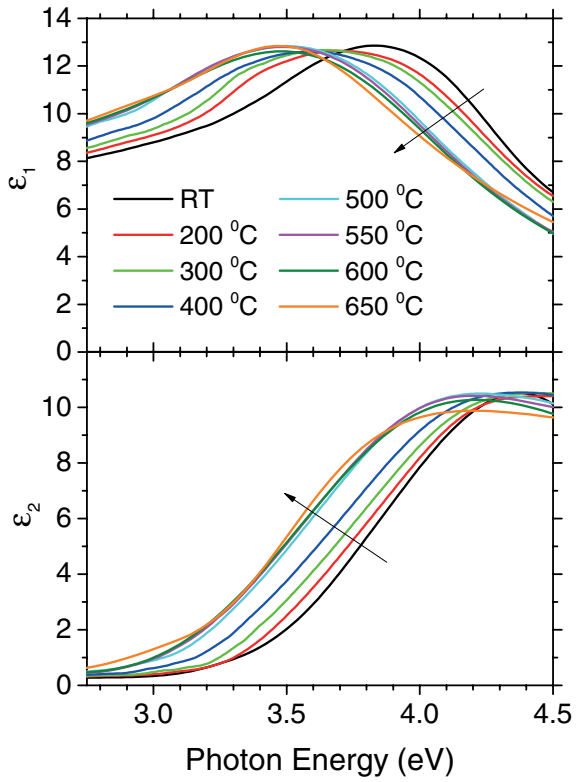

Figure 2. The temperature dependence of the real and imaginary part of the dielectric function at the photon energy range close to the band gap. The arrows show increasing temperature.

given in the literature [13]. The substrate parameters were then kept fixed in the further fitting, where the parameters of the $PbTiO_3$ film were determined. To get good agreement between the calculated spectrum and experimental data, we had to include a surface roughness of the film (∼5 nm) and an intermix (∼3 nm) layer between the $PbTiO_3$ film and Al_2O_3 substrate into our structural (geometric) model. The dielectric function for both interface layers was determined as a mixture of two adjacent layers using the effective medium approximation. The surface roughness was measured by a surface profiler and its value was found to be of 5 nm and in good agreement with the calculated value.

The dielectric function of the $PbTiO_3$ layer was determined in several steps. First, the film thickness and its refractive index were calculated in the transparent spectral region below the band edge. The dielectric function in this region is real and its imaginary part is zero or negligibly small. The refractive index and film thickness can be easily obtained by reversing ellipsometric data or using the familiar Cauchy–Urbach dispersion formula. The total film thickness evaluated in this way agrees with the nominal value given by deposition conditions and with the value measured by a surface profiler (alpha step). After that, the dielectric function was calculated in the entire spectral region including the non-transparent region above the band gap, with the film thickness fixed and taken from previous calculation. The $PbTiO_3$ film parameters were determined by modeling the spectra by other dispersion models (the Tauc–Lorentz [14] and Cody–Lorentz [15]). The final spectrum adjustment was done using the so-called point-to-point fit.

Figure 2 exhibits the real and imaginary parts of the dielectric function $\varepsilon_1(E)$ and $\varepsilon_2(E)$ depending on photon energy at various temperatures, which were extracted from the ellipsometric data by the above-mentioned fitting procedure. The spectra are calculated in the vicinity of the band gap for selected temperatures from room temperature to 950 K. The variation of the band gap with temperature is demonstrated by the increase in the ε_2 and corresponding ε_1 variation to lower energy with increasing temperature. The peaks in dielectric function are usually assigned to the transitions between critical points or lines in the Brillouin zone referred to as van Hove singularities. In our case the anomalies in ε_1 and ε_2 are connected with the electron transitions between the valence and conduction bands of $PbTiO_3$ thin film and indicate the band gap. The spectra show very clearly a shift of the absorption edge, and therefore, also the band gap to lower energies with increasing temperature. The absorption coefficient α is closely related to the imaginary part of the dielectric function ε_2 as $\alpha = \omega\varepsilon_2/cn$. The band gap was determined supposing the parabolic band densities of states (DOS). The magnitude of the band gap was deduced from the Tauc plot of $(\alpha n/E)^2$ versus E (photon energy) for constant momentum matrix elements and the Cody plot $(\alpha nE)^2$ versus E for constant dipole matrix elements, where n is the refractive index. In both plots the intersection of its linear extrapolation with the energy axis gives the value of the band gap.

The temperature dependence of the band gap determined by the above-mentioned method is plotted in figure 3(a). The band gap varies from the value 3.88 eV at room temperature

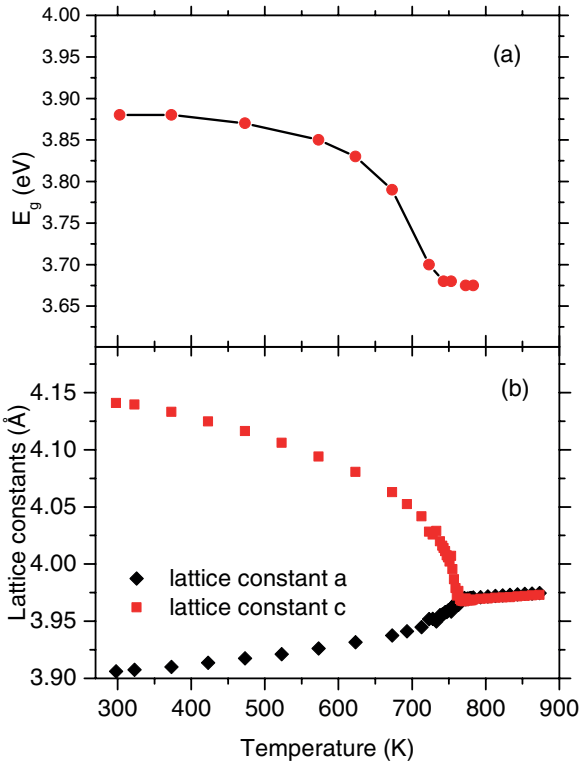

Figure 3. The temperature dependence of the band gap E_g (panel (a)) and temperature dependence of the lattice parameters (panel (b)).

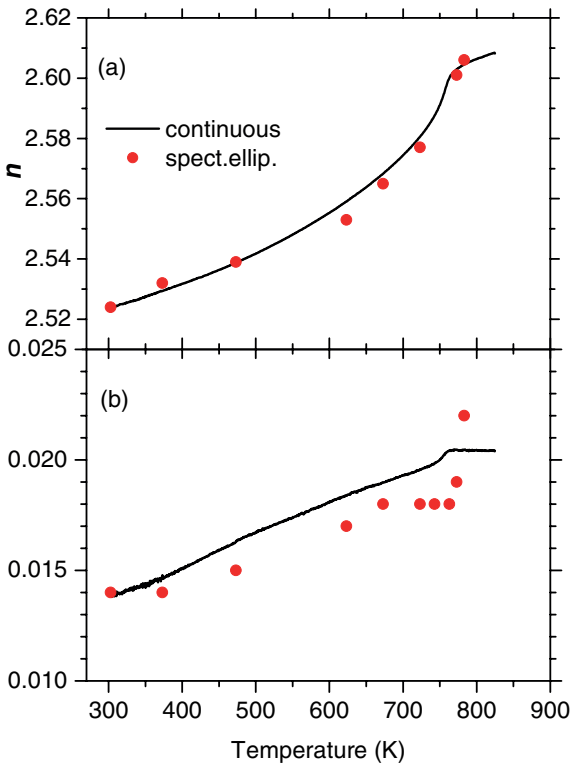

Figure 4. The temperature dependence of the refractive index n and extinction coefficient κ at 1.5 eV (below the band gap E_g) compared with the data calculated from spectroscopic ellipsometry.

to the value 3.67 eV just below the phase transition and then varies only slightly. In panel (b) the temperature dependence of the lattice parameters obtained by XRD is shown for comparison. Strong correlation in temperature dependence can be seen in both graphs.

The changes of lattice constants and relative displacement of atoms modify the electronic structure and optical response functions. In order to identify the phase transition in $PbTiO_3$ independently from its optical properties we carried out the measurement of the temperature dependence of the refractive index. The complex refractive index, $\tilde{N} = n + ik$, is related to the dielectric function by $n = [(\varepsilon_1^2 + \varepsilon_2^2)^{1/2} + \varepsilon_1]^{1/2}/\sqrt{2}$, $k = [(\varepsilon_1^2 + \varepsilon_2^2)^{1/2} - \varepsilon_1]^{1/2}/\sqrt{2}$, where n is the refractive index and k is the extinction coefficient. To determine $\tilde{N}$ we set our spectroscopic ellipsometer at the energy 1.5 eV (deep below E_g) and keeping it fixed we varied the temperature continuously from room temperature up to 850 K. The real and imaginary part of the refractive index were calculated using the Cauchy–Urbach model. The resulting plot of the refractive index versus temperature is given in figure 4, which in addition shows the data calculated from spectroscopic ellipsometry for comparison. Very similar dependence has been published using a He–Ne laser [16] on a $PbTiO_3$ single crystal. They also show that the refractive index along the c-axis and perpendicular to it vary in nearly the same way showing that the optical anisotropy is very small in contrast to very strong anisotropy in lattice parameters. This also explains the fact that our data on the polycrystalline film are similar to those taken on single crystals.

4. Theoretical calculations

The electronic structures and optical properties of $PbTiO_3$ can be determined by the photon–energy dependent dielectric function $\tilde{\varepsilon}(E) = \varepsilon_1(E) + i\varepsilon_2(E)$ that is mainly connected with the electronic structures respective with the critical points in the DOS. The imaginary part $\varepsilon_2(E)$ of the dielectric function $\tilde{\varepsilon}(E)$ can be calculated from the momentum matrix elements between the occupied and unoccupied states within the selection rules. Some recent calculations can be found in the literature [17–19].

The first principle calculations were performed using the standard full potential linear augmented plane wave code Wien2k [20] or the VASP-PAW [21] program package using the projector augmented wave scheme [22]. For our dielectric function calculations we used the values of the lattice constants $a_{RT} = 3.904$ Å, $c_{RT} = 4.152$ Å for the tetragonal phase and $a_{cub} = 3.960$ Å for the cubic phase. The energy difference E_{cubic}–$E_{tetragonal} \approx 60$ meV per unit cell and approximatively corresponds to 720 K which is not very far from $T_c = 766$ K.

The linear response of the system to an electromagnetic field is given through the complex dielectric function $\tilde{\varepsilon}(\omega)$. We consider here only the electronic excitations.

$$\varepsilon_2(E) = [2e^2\pi/(\Omega\,\varepsilon_0)] \sum_{k,v,c} |\langle\psi_k^c|u.r|\psi_k^v\rangle|^2\,\delta(E_k^c - E_k^v - E) \qquad (1)$$

where E is photon energy and e is the electronic charge. ψ_k^c and ψ_k^v are the conduction and valence band wavefunctions at k, respectively. The real part $\varepsilon_1(E)$ of the dielectric function $\tilde{\varepsilon}(E)$ can be derived from the imaginary part $\varepsilon_2(E)$ using the

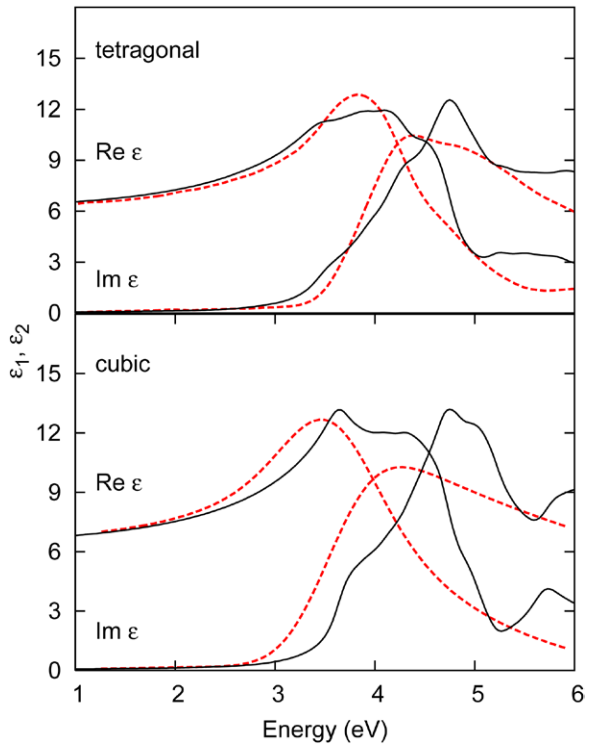

Figure 5. The complex dielectric function of $PbTiO_3$. The red and dashed curves were determined using spectroscopic ellipsometry and the black ones were found from band structure calculation. To correct the gap theoretical curves were shifted by 0.4/1.0 eV for the tetragonal/cubic phase.

Kramers–Kronig dispersion equation. All other optical constants can be derived from $\varepsilon_1(\omega)$ and $\varepsilon_2(\omega)$.

The optical functions were evaluated using the Wien2k package [20]. In all calculations the generalized gradient approximation [23] has been employed. We obtained the value 2.9 eV for the direct gap and 1.5 eV for the indirect one. There is a well-known bandgap problem in DFT that underestimates the band gap and this is the reason why the agreement between the experimental and calculated values of the dielectric permittivity tensor is often unsatisfactory. A possible and simple method to alleviate this problem is to introduce a scissors operator Λ_{xc}, as described, for example, by Levine and Allan [24]. In this approximation the conduction bands are shifted by a constant to fit the experimental data. More sophisticated solutions of this problem can be obtained by using some approximations of many body theory (e.g. GW approximation).

Figure 5 shows the complex dielectric function $\tilde{\varepsilon}(E) = \varepsilon_1(E) + i\varepsilon_2(E)$ of both, calculated and determined from our spectroscopic ellipsometry measurements. The difference between the calculated and experimental spectra was corrected using the scissors operator and the most suitable scissors value to fit the main absorption peak was 0.4 eV for the tetragonal and 1.0 eV for the cubic phase. The optical spectra in figure 5 were calculated with a 50 meV broadening. The spectra were averaged with respect to the polarization of the electric field, $\vec{E}$, parallel and perpendicular to the c-axis to better reflect our experimental data obtained on polycrystalline films.

Table 1. Relative position shifts of individual atoms in the z-direction related to the O_6 octahedron in Å.

	Exp. [7]	Exp. [26]	Our calculation
Δz_{Ti}	0.30	0.31	0.31
Δz_{Pb}	0.47	0.49	0.44

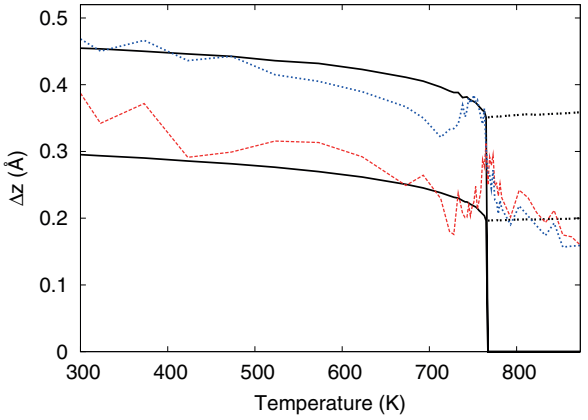

Figure 6. The temperature dependence of the Pb and Ti shifts related to the O_6 octahedron. The black solid lines result from theoretical simulation and the color dotted lines are experimental x-ray data. The black dotted lines were obtained with $a = c$ and Δz not constrained.

During the theoretical study of the optical properties of $PbTiO_3$ films we noticed several other interesting characteristic features. We could simulate the temperature dependence of the electronic structure and optical properties using the structural data obtained at various temperatures as the input data for our calculations. Minimizing the atomic forces, we calculated the Δz parameters describing the deviation of the Ti and Pb atoms with respect to the center of gravity of the oxygen octahedron along the z-axis. The results for a_{RT}, c_{RT} are presented in table 1 and are in good agreement with our x-ray measured values and literature [7, 25].

Figure 6 shows the temperature dependence of the deviation of the atomic positions Δz from their high-symmetry cubic positions, where $\Delta z = 0$ for Pb and Ti. The steep drop in the measured Δz also indicates that the phase transition is of the first order. The values for Δz were calculated in this way for temperature varying from room temperature to 850 K by minimizing the atomic forces acting on individual atoms. Comparing our x-ray data and calculation results, there is good agreement for temperatures below T_c. For temperatures above T_c, however, the x-ray Δz values drop steeply to zero but the calculated values remain practically on the same level. To obtain the same drop also for the calculated Δz it is not sufficient to set the a and c lattice parameters to be equal but the cubic symmetry must be enforced by setting all $\Delta z = 0$. When this constraint is released the system prefers the tetragonal symmetry and the calculated Δz remains nonzero in our simulation also above T_c. This is a simple consequence that our calculations always give lower energy for the distorted phase than for the cubic one. In reality, this happens most probably only at a short-range scale, and the observed cubic symmetry is restored due to the long-range averaging. This finding

seems to be in perfect agreement with the experimental work of Sicron *et al* [8] who observed the atomic distortions in the high-temperature phase and proposed that they are due to a local instability of the cubic structure.

A reason for this may be a strong tendency to covalent instead of pure ionic bonding in $PbTiO_3$ [9]. As recently shown in [26], the formation of partly covalent Pb–O bonds is a characteristic feature of the tetragonal phase of $PbTiO_3$. Another mechanism based on the hybridization between the titanium 3d and oxygen 2p states is also essential for ferroelectricity in $BaTiO_3$ and leads to large strain that stabilizes the tetragonal symmetry [27]. However, the resulting off-centering is at a local level and does not say whether the local distortions line up to form a ferroelectric phase.

As the ground state of $PbTiO_3$ is of tetragonal symmetry, the atomic distortion at low temperatures, below T_c, is uniform and of a long-range nature, and leads to a structural ordering corresponding to a ferroelectric phase and gives a rise of macroscopic polarization. As the temperature increases, clusters with different polarization orientation appear and their volume increases on heating. At T_c the macroscopic polarization steeply vanishes but a local distortion locally remains of what was observed by using x-ray absorption fine structure (XAFS) measurements [8]. This behavior is similar to the eight-sites or order-disorder model for $BaTiO_3$ and $KNbO_3$ [28, 29]. On the other hand, this model cannot account for the observed phonon softening, which was observed by many experimental techniques [30] and prefers the displacive character of the transition. Near the transition temperature a central peak was observed [31], which is interpreted as a manifestation of disorder in the system. Neutron diffraction experiments also suggest that $PbTiO_3$ has a certain degree of disordered distortions above the phase transition [32]. Furthermore, the magnitude of its dielectric constant was found to be larger than that expected from the Lyddane–Sachs–Teller relation suggesting the ordinary displacive-type model. There is a long controversy on this topic [33]. However, the order-disorder and soft-mode pictures are not mutually exclusive [34] and there is a suggested crossover [31] from displacive to order–disorder behavior near the phase transition temperature. The pure soft-mode model and the eight-site model can be considered as limiting cases and most of the experimental data are consistent with their combination. Their theoretical compatibility was achieved by introducing a linear coupling between the pseudospins representing the local distortion and the transverse optic soft mode [35].

The phase transition in $PbTiO_3$ is of first-order character what means that the thermodynamic potential in the frame of the Landau theory must be expanded up to the sixth order [6]. In this case the thermodynamic potential shows subsidiary minima corresponding to the locally distorted tetragonal phase. The relatively high temperature at which the phase transition takes place allows for the fluctuations among them and the phase transition shows some features of an order–disorder model. The disorder, which is in this way introduced in this material, is responsible for the enhanced role which the Urbach tail plays in our spectra in comparison to classical semiconductors.

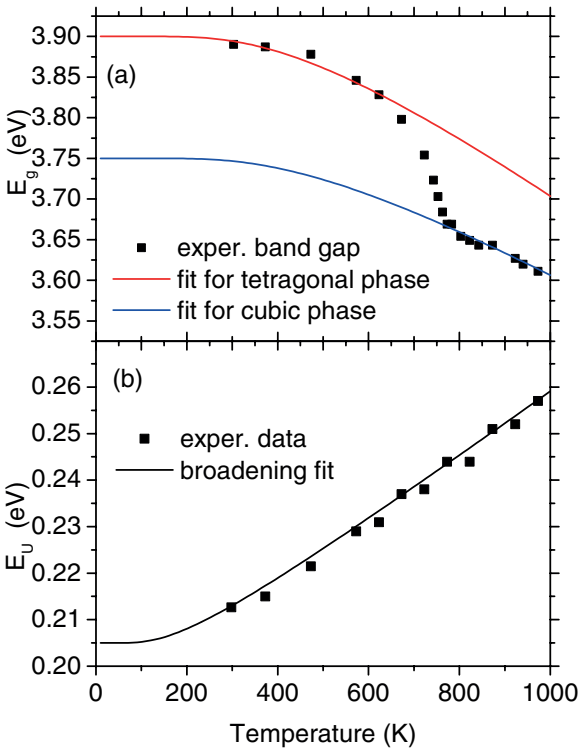

Figure 7. The temperature dependence of the band gap (a) and the Urbach tail (b). The temperature dependence is fit by equations (3) and (2), respectively.

The figures 3 and 7 show continuous behavior in the vicinity of the phase transition comparing it with a steeper rise in the case of single crystals [12]. This is caused by the polycrystalline film character and the influence of the substrate, which has different thermal expansion characteristics than the deposited film. Both factors smear the difference between the characteristic behavior of the first and order transitions.

We can conclude that our calculations give preference to the distorted ground state, which is realized by the redistribution of charge among ions due to p–d hybridization. The resulting local distortion plays an important role in understanding the temperature dependence of the band gap and the temperature behavior of our ellipsometric spectra. In this way our optical spectra of $PbTiO_3$ show some features which support the previous XAFS measurements and some conclusions about the nature of the phase transition following from them.

5. Discussion

Studying the imaginary part ε_2 in figure 2 it can be noted that it slowly increases with increasing photon energy below the band gap. This increase is caused by several mechanisms. First-principle calculations show that $PbTiO_3$ is an indirect band gap material. This was theoretically confirmed by several authors [17, 18, 36] including this paper. The scissors corrected absorption coefficient for this mechanism is very low, typically $<10^2\text{cm}^{-1}$, and it starts at 3.30 eV as follows from our calculation. The absorption in this case is described by the formula $\varepsilon_2 \propto (E \mp E_p - E_g)^2$, where E_p is the energy of the partaken phonon.

Furthermore, the absorption edge in perovskites is significantly broadened by an exponential tail which extends over an energy range of 0.1–0.5 eV [37, 38]. Its existence causes an experimental complication in determining the exact position of the band gap. The absorption coefficient in this energy interval varies from 10^2 to 10^4 cm^{-1}. This effect is called the Urbach tail and was first observed in the silver and alkali halides [39]. It is also often observed in many crystalline and amorphous materials [40] suggesting that the Urbach absorption is a nearly universal property of solids. Several models were put forward to explain its origin but it remains still unexplained. A dominant role is played by thermal and structural disorder giving temperature dependent and independent contribution, respectively. In perovskite it was first reported in [37] and then it was indicated in all perovskites [41]. The absorption coefficient is typically described by the following expression [42].

$$\alpha(E) = \alpha_0 \exp(E/E_U(T)), \text{ where}$$
$$E_U(T) = E_U(0) + a_U/[\exp(\Theta_U/T) - 1] \quad (2)$$

Here, α_0, $E_U(0)$ a_U and Θ_U are fitting parameters with $E_U(T)$ representing the steepness of the absorption edge and $E_U(0)$ is a contribution from static disorder.

The contributions from the indirect gap and Urbach tail overlap with the direct electronic transitions, which start at the minimum, M_0, in the joint DOS obtained from first principle calculation. This is the reason why it is difficult to observe the indirect transition or onset of direct transition, because they are hidden by the strong Urbach tail. Therefore, we determine the direct band gap in the frequency range where the value of the absorption coefficient is higher $\sim 10^4$ cm^{-1} and is not influenced by the other mechanisms.

For understanding what is going on in such materials it is necessary to study the temperature dependence of optical properties. The temperature dependence of electronic band states can be separated into two competing contributions [43]. One contribution arises from the thermal expansion of the lattice and the second one is due to the renormalization of the band structure by electron–phonon interaction. These two contributions [44] are responsible for the magnitude and the sign of the thermo-optic coefficient $\partial n/\partial T$. It is negative if the first mechanism dominates and is positive in the opposite case. The electron–phonon interaction results in a complex, frequency dependent self-energy $\Sigma = \Sigma_r + i\Sigma_i$, which describes the shift and broadening of energy levels. In the case of perovskites the self-energy effects can be phenomenologically handled by the Bose–Einstein factors. The thermal expansion has been estimated for $PbTiO_3$ and is of order 1×10^{-6} K^{-1} [45] similarly as for most of the semiconductors [46]. In the case of semiconductors there are attempts to distinguish these two contributions [44]. For perovskites the situation is more complex (more phonons and complex electronic structure) and since both contributions have very similar temperature dependences, it is not necessary to distinguish them and the use of a simple (phenomenological) fitting equation is justified [47].

The temperature dependence of the band gap can be described using the phenomenological Bose–Einstein model, which can describe the thermal band shrinking, transition broadening and tail band behavior. First, we confine ourselves to the band gap variation. The model consists of two branches described by equation (3), which correspond to the band gap temperature dependence below and above T_C, respectively and can be expressed as

$$E_g(T) = E_g(0) - 2a_g/[\exp(\Theta_g/T) - 1] \quad (3)$$

where $E_g(0)$ is the band gap energy extrapolated to $T = 0$ K, a_g is a temperature-independent constant corresponding to the strength of electron–phonon coupling, Θ_g is the average phonon temperature and T is the experimental temperature. The values of the fit parameters are: $E_g(0) = 3.9$ eV, $a_g = 300$ meV and $\Theta_g = 1400$ K for the tetragonal phase and $E_g(0) = 3.75$ eV, $a_g = 250$ meV and $\Theta_g = 1500$ K for the cubic phase. They are much higher than the data for GaAs ($a_g = 57$ meV, $\Theta_g = 240$ K) [48]. On the other hand they are much more comparable with wide band materials GaN (158 meV and 564 K) and AlN (670 meV and 1000 K) [49]. An extensive review of this topic with many examples of semiconducting materials is given in [43].

Figure 7(a) shows the temperature dependence of the band gap in our $PbTiO_3$ films and the fit of the data using equation (3). It can be seen that there is a low-temperature region corresponding to the band gap in the tetragonal phase, then there is a transient region around T_c and finally the range of temperatures corresponding to the cubic phase. The temperature dependence in both tetragonal and cubic phases can be fitted by equation (3) with different parameters. Similar analysis can be done for the temperature dependence of Urbach tail fitting the exponential dependence of the absorption coefficient below the gap. Using equation (2), the results are shown in figure 7(b). A relatively small increase with temperature is seen. The thermal fluctuation forms about 17% in the entire temperature interval. This demonstrates that temperature dependent contribution is much smaller than $E_U(0) = 205$ meV saying that the Urbach tail is mainly formed by static disorder.

6. Conclusions

The XRD confirmed the polycrystalline nature and pure perovskite structure of $PbTiO_3$ thin films prepared by the CSD technique. Using the same technique we measured their lattice parameters in the temperature range from room temperature to 950 K. We also measured ellipsometric spectra and using several methods we extracted their dielectric function and other optical response functions in the same temperature range as XRD. The optical properties were calculated from first principles for cubic and tetragonal phases. Comparing the results of the temperature dependence of optical and structural properties for $PbTiO_3$ thin films a strong correlation was found between them. Small temperature variation of the optical band gap far from the phase transition becomes dramatically close to the phase transition temperature, where also the lattice parameters vary strongly. The optical band gap reduces in the cubic high-temperature phase, which

forms above the temperature where the anisotropic ratio *c*/*a* shows a typical splitting. At this temperature an anomaly in the behavior of real and imaginary parts of the refractive index are observed.

Results of our *ab initio* calculations are in reasonable agreement with experimental findings, although they are based on a simplified model in which the temperature variations are represented only via temperature dependent lattice constants. This approximation seems to be justified for materials with the displacive nature of the phase transitions, with an exception of the close vicinity of the critical point where the fluctuation cannot be neglected. Our calculations also lead to the revision of a simple view on the behavior of $PbTiO_3$. It was shown that the distorted phase always has lower energy than the cubic one and the tetragonal distortion survives also for temperatures above T_C, at least locally. This is in agreement with the XAFS experiment [8] and interpreted in the terms of theory [35]. By simulating the temperature dependence of the band gap we show that off-center local ion displacement plays an important role in its understanding.

Acknowledgment

This work was supported in part by the Grant Agency of the Czech Republic under Contract No. 204/11/1011. Access to computing facilities provided by the National Grid Infrastructure MetaCentrum under the program LM2010005 is greatly appreciated.

References

[1] Moulson A and Herbert J 2003 *Electroceramics* 2nd edn (New York: Wiley)
[2] Xu Y 1991 *Ferroelectric Materials and Their Applications* (New York: North-Holland)
[3] Jacobson A J 2009 *Chem. Mater.* **22** 660–74
[4] Fu H and Cohen R E 2000 *Nature* **403** 281–3
[5] Jona F and Shirane G 1993 *Ferroelectric Crystals* (New York: Dover Publications)
[6] Lines M and Glass A 1977 *Principles and Application of Ferroelectrics and Related Materials* (Oxford: Clarendon)
[7] Shirane G, Pepinsky R and Fraze B C 1956 *Acta Crystallogr.* **9** 131
[8] Sicron N, Ravel B, Yacoby Y, Stern E A, Dogan F and Rehr J J 1994 *Phys. Rev.* B **50** 13168–80
[9] Rabe K and Waghmare U 1996 *J. Phys. Chem. Solids* **57** 1397 (*Proc. of the 3rd Williamsburg Workshop on Fundamental Experiments on Ferroelectrics*)
[10] Huang Y H 1995 Sol-gel $PbTiO_3$ thin films for pyroelectric applications EPFL thèse no 1343
[11] Šimek D, Kužel R and Rafaja D 2006 *J. Appl. Crystallogr.* **39** 487–501
[12] Mabud S A and Glazer A M 1979 *J. Appl. Crystallogr.* **12** 49–53
[13] Gervais F 1998 Aluminium oxide (Al_2O_3) *Handbook of Optical Constants of Solids* vol **2**, ed E D Palik (New York: Academic) p 761
[14] Jellison G E and Modine F A 1996 *Appl. Phys. Lett.* **69** 2137
[15] Ferlauto A S, Ferreira G M, Pearce J M, Wronski C R, Collins R W, Deng X and Ganguly G 2002 *J. Appl. Phys.* **92** 2424–36
[16] Kleemann W, Schäfer F J and Rytz D 1986 *Phys. Rev.* B **34** 7873–9
[17] Hosseini S M, Movlarooy T and Kompany A 2005 *Eur. Phys. J.* **46** 463–9
[18] Hosseini S, Movlarooy T and Kompany A 2007 *Physica* B **391** 316–21
[19] Hermet P, Veithen M and Ghosez P 2009 *J. Phys.: Condens. Matter* **21** 215901
[20] Blaha P, Schwarz K, Madsenand G, Kvasnicka D and Luitz J 2001 *WIEN2k, An Augmented Plane Wave + Local Orbitals Program for Calculating Crystal Properties* (Techn. Universität, Wien: Karlheinz Schwarz)
[21] Kresse G and Furthmüller J 1996 *Phys. Rev.* B **54** 11169–86
[22] Kresse G and Joubert D 1999 *Phys. Rev.* B **59** 1758–75
[23] Perdew J P, Burke K and Ernzerhof M 1996 *Phys. Rev. Lett.* **77** 3865–8
[24] Levine Z H and Allan D C 1989 *Phys. Rev. Lett.* **63** 1719–22
[25] Glazer A M and Mabud S A 1978 *Acta Crystallogr.* B **34** 1065–70
[26] Kuroiwa Y, Aoyagi S, Sawada A, Harada J, Nishibori E, Takata M and Sakata M 2001 *Phys. Rev. Lett.* **87** 217601
[27] Cohen R E 1992 *Nature* **358** 136
[28] Dougherty T P, Wiederrecht G P, Nelson K A, Garrett M H, Jensen H P and Warde C 1992 *Science* **258** 770–4 www.jstor.org/stable/2880323
[29] Dougherty T P, Wiederrecht G P, Nelson K A, Garrett M H, Jenssen H P and Warde C 1994 *Phys. Rev.* B **50** 8996–9019
[30] Scott J F 1974 *Rev. Mod. Phys.* **46** 83–128
[31] Fontana M, Wojcik K, Idrissi H and Kugel G 1990 *Ferroelectrics* **107** 91–6
[32] Nelmes R and Kuhs W 1985 *Solid State Commun.* **54** 721–3
[33] Comes R, Lambert M and Guinier A 1968 *Solid State Commun.* **6** 715–9
[34] Müller K, Luspin Y, Servoin J and Gervais F 1982 *J. Phys. Lett.* **43** 537–42
[35] Pirc R and Blinc R 2004 *Phys. Rev.* B **70** 134107
[36] Piskunov S, Heifets E, Eglitis R and Borstel G 2004 *Comput. Mater. Sci.* **29** 165–78
[37] DiDomenico M and Wemple S H 1968 *Phys. Rev.* **166** 565
[38] Wemple S H 1970 *Phys. Rev.* B **2** 2679–89
[39] Urbach F 1953 *Phys. Rev.* **92** 1324
[40] Tauc J, Grigorovici R and Vancu A 1966 *Phys. Status Solidi* **15** 627
[41] Capizzi M and Frova A 1970 *Phys. Rev. Lett.* **25** 1298–302
[42] Cody G D, Tiedje T, Abeles B, Brooks B and Goldstein Y 1981 *Phys. Rev. Lett.* **47** 1480
[43] Cardona M and Thewalt M L W 2005 *Rev. Mod. Phys.* **77** 1173–224
[44] Bhosale J, Ramdas A K, Burger A, Muñoz A, Romero A H, Cardona M, Lauck R and Kremer R K 2012 *Phys. Rev.* B **86** 195208
[45] Taylor T R, Hansen P J, Acikel B, Pervez N, York R A, Streiffer S K and Speck J S 2002 *Appl. Phys. Lett.* **80** 1978
[46] Yang J, Gao Y, Wu J, Huang Z, Meng X, Shen M, Sun J and Chu J 2010 *J. Appl. Phys.* **108** 114102
[47] O'Donnell K P and Chen X 1991 *Appl. Phys. Lett.* **58** 2924
[48] Lautenschlager P, Garriga M, Logothetidis S and Cardona M 1987 *Phys. Rev.* B **35** 9174
[49] Nam K B, Li J, Lin J Y and Jiang H X 2004 *Appl. Phys. Lett.* **85** 3489